Cell Reports, Volume *20*

Supplemental Information

Deletion of *Nampt* in Projection Neurons of Adult Mice Leads to Motor Dysfunction, Neurodegeneration, and Death

Xiaowan Wang, Qiao Zhang, Ruisi Bao, Nannan Zhang, Yingzhen Wang, Luis Polo-Parada, Andrew Tarim, Aidan Alemifar, Xianlin Han, Heather M. Wilkins, Russell H. Swerdlow, Xinglong Wang, and Shinghua Ding

SUPPLEMENTAL INFORMATION

Neuronal Deletion of *Nampt* in Adult Mice Leads to Motor Dysfunction, Neurodegeneration and Death

Xiaowan Wang, Qiao Zhang, Ruisi Bao, Nannan Zhang, Luis Polo-Parada, Andrew Tarim, Aidan Alemifar, Xianlin Han, Heather M. Wilkins, Russell H. Swerdlow, Xinglong Wang, Shinghua Ding*

*Corresponding author

Inventory of Supplemental Information

Supplemental Figures S1-S7

Supplemental Experimental Procedures

Supplemental Figures

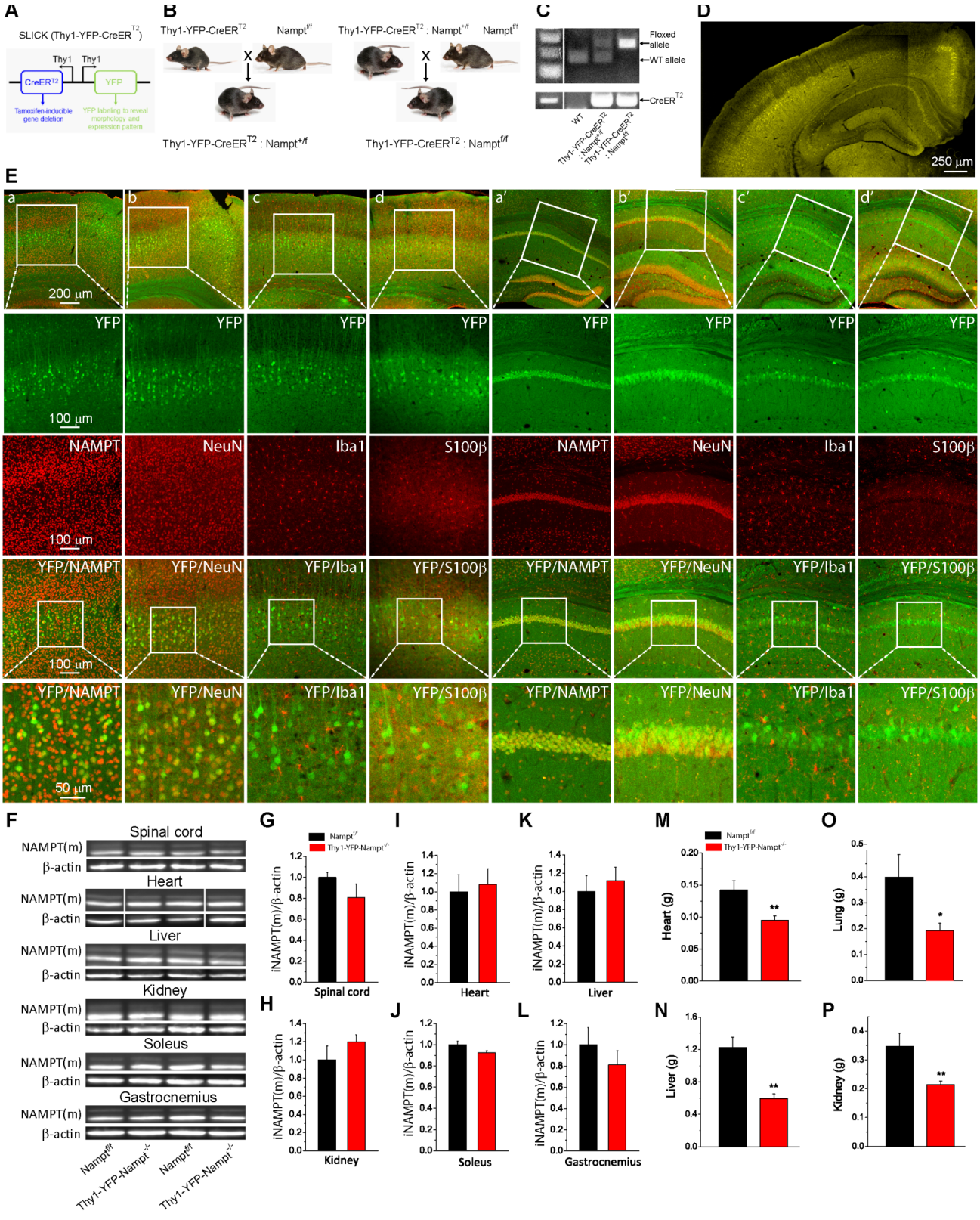

Figure S1. Generation of projection neuron-specific and inducible *Nampt* cKO mice and transgene expression pattern (Related to Figure 1). (A) Schematic representation of Single-neuron Labeling with Inducible Cre-mediated Knockout (SLICK) H line of transgenic mice (Young et al., 2008). Two copies of the Thy1 promoter drive expression of YFP and the inducible form of Cre recombinase, $CreER^{T2}$. (B) Scheme for mouse breeding to generate $Nampt^{+/f}$:*Thy1-YFP-*$CreER^{T2}$ and $Nampt^{f/f}$:*Thy1-YFP-*$CreER^{T2}$ transgenic mice. (C) Genotyping results. The DNA marker image (left) was stitched indicated by the white line. (D) Fluorescent images of YFP expression in the cortex and hippocampus of *Thy1-YFP-*$CreER^{T2}$ mice. The expression of YFP and $CreER^{T2}$ in *Thy1-YFP-*$CreER^{T2}$ mice was highly correlated with a ratio of more than 96% (Young et al., 2008). (E) Immunofluorescent images showing YFP expression and immunofluorescence of NAMPT, NeuN, Iba1 and S100β in the cortex (a-d) and hippocampus (a'-d'). The top panels are epi-fluorescent images and lower panels are confocal images. The lower panels are the high-resolution images of the boxed regions in the upper panels. Notice that YFP was primarily expressed in NeuN+ neurons, and was absent in Iba1+ microglia and S100β+ astrocytes in the cortex and hippocampus of the *Thy1-YFP-*$CreER^{T2}$ mice. (F) Western blots for NAMPT using mouse anti-NAMPT antibody. The white lines indicate the sliced images. (G-L) Summary data of iNAMPT expression in spinal cord (G), kidney (H), heart (I), soleus (J), liver (K) and gastrocnemius (L). Notice that iNAMPT protein expression levels remained unchanged in non-CNS organs of *Thy1-YFP-*$Nampt^{-/-}$ cKO mice as compared with $Nampt^{f/f}$ mice. In (G-L), N = 4 mice for each genotype. (M-P) The effect of homozygous *Nampt* deletion in the projection neurons on the weights of the non-CNS organs including heart (M), lung (N), liver (O) (and kidney (P). The organs were collected three weeks after TAM administration. N = 6 for $Nampt^{f/f}$ mice and N = 8 for *Thy1-YFP-*$Nampt^{-/-}$ cKO mice. $*P < 0.05$, $**P < 0.01$, t-test. Error bars represent ±SEM.

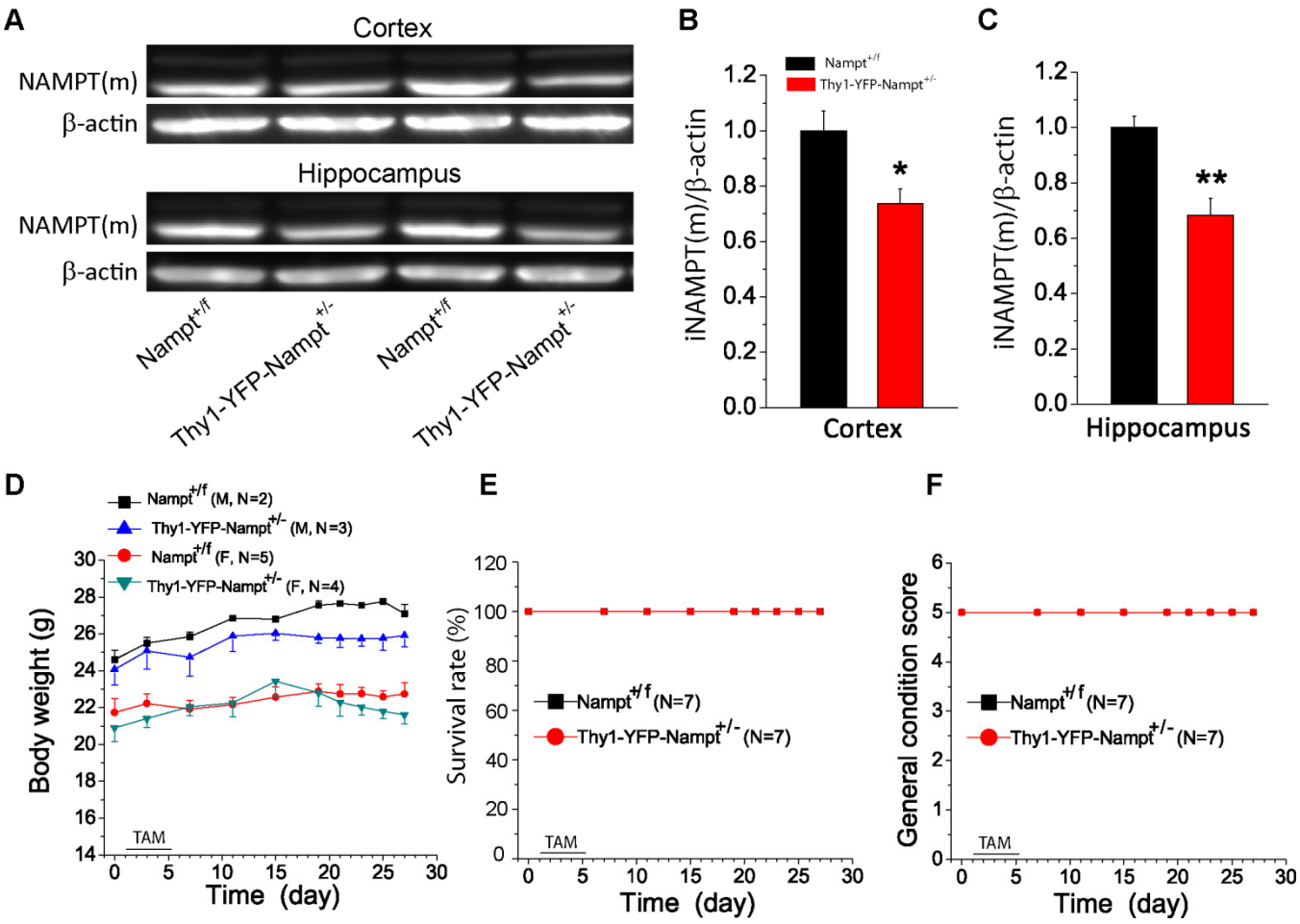

Figure S2. Heterozygous deletion of *Nampt* in the projection neurons (Related to Figure 1 and 2). (A) Western blots for cortical and hippocampal NAMPT and β-actin in the *Nampt*$^{+/f}$ mice and *Thy1-YFP-Nampt*$^{+/-}$ cKO mice. β-actin was used as an equal loading control. (B-C) Summary data of relative cortical and hippocampal NAMPT expression levels in the *Nampt*$^{+/f}$ mice and *Thy1-YFP-Nampt*$^{+/-}$ cKO mice. Notice that the NAMPT expression levels were reduced in *Thy1-YFP-Nampt*$^{+/-}$ cKO mice. N=4 mice for each genotype. *$P < 0.05$, **$P < 0.01$, t-test. Time courses of body weight (D), survival rate (E) and general condition scores (F) for *Nampt*$^{+/f}$ mice and *Thy1-YFP-Nampt*$^{+/-}$ cKO mice. Error bars represent ±SEM.

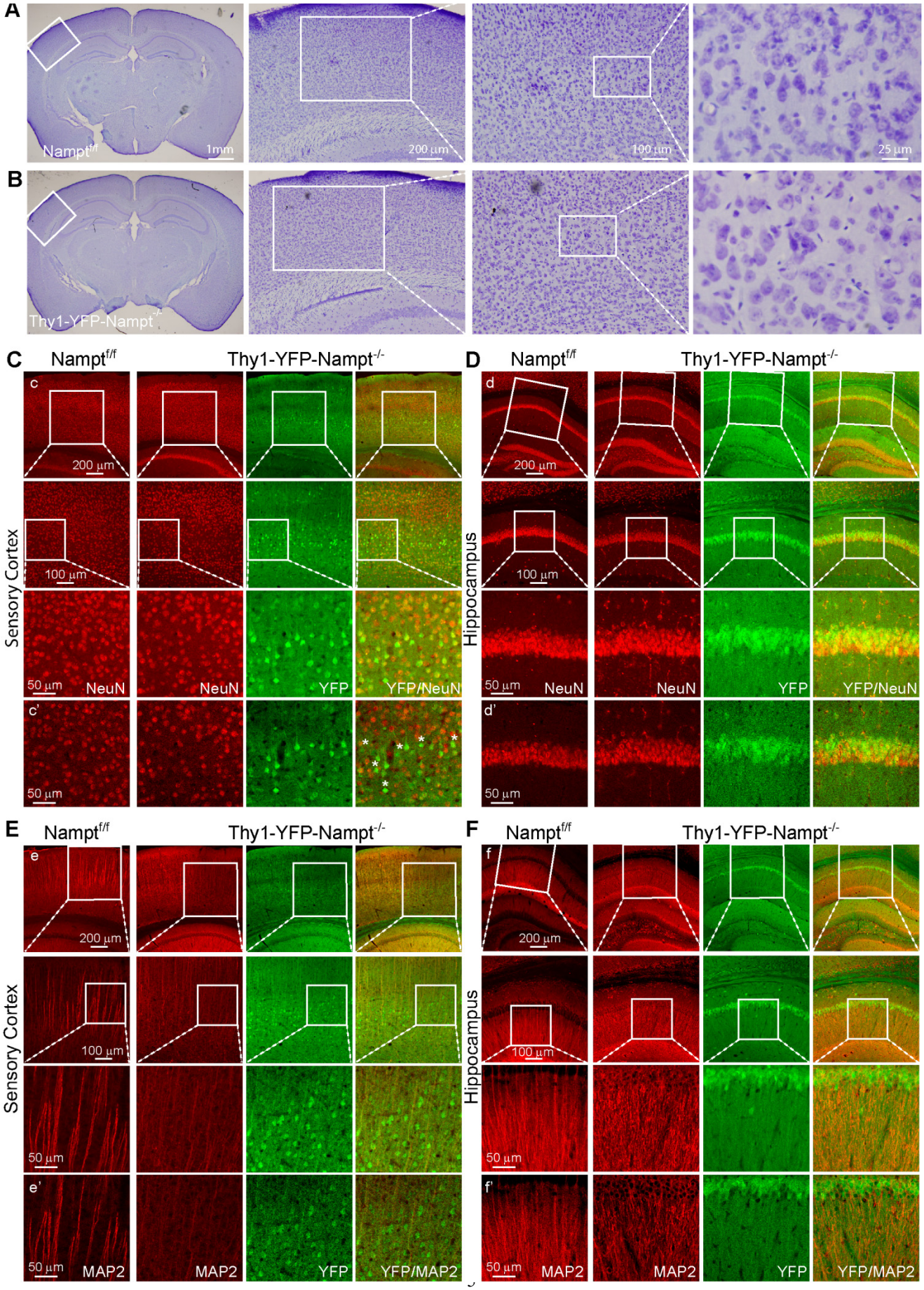
A
Nampt f/f
1mm
200 μm
100 μm
25 μm
B
Thy1-YFP-Nampt -/-
C
Nampt f/f
Thy1-YFP-Nampt -/-
c
200 μm
100 μm
Sensory Cortex
50 μm
NeuN
NeuN
YFP
YFP/NeuN
c'
50 μm
D
Nampt f/f
Thy1-YFP-Nampt -/-
d
200 μm
100 μm
Hippocampus
50 μm
NeuN
NeuN
YFP
YFP/NeuN
d'
50 μm
E
Nampt f/f
Thy1-YFP-Nampt -/-
e
200 μm
100 μm
Sensory Cortex
50 μm
e'
50 μm
MAP2
MAP2
YFP
YFP/MAP2
F
Nampt f/f
Thy1-YFP-Nampt -/-
f
200 μm
100 μm
Hippocampus
50 μm
f'
50 μm
MAP2
MAP2
YFP
YFP/MAP2

Figure S3. *Thy1-YFP-Nampt*$^{-/-}$ cKO mice exhibit neuronal loss and dendritic lesion in the sensory cortex (Related to Figure 3). (A-B) Representative Nissl staining images of coronal brain sections including the sensory cortices of *Nampt*$^{f/f}$ and *Thy1-YFP-Nampt*$^{-/-}$ mice. Right panels are high-resolution images of the boxed regions in the left panels. (C-D) Representative confocal images in the sensory cortex and hippocampus of *Nampt*$^{f/f}$ and *Thy1-YFP-Nampt*$^{-/-}$ mice stained with neuron-specific marker NeuN. Lower panels are high-resolution images of the boxed regions in the upper panels. c-d) Confocal maximal projection images (top). c'-d') Confocal single frame images (bottom). Notice that many of YFP+ cells are NeuN- (indicated by white stars) in the sensory cortex of *Thy1-YFP-Nampt*$^{-/-}$ cKO mice. (E-F) Representative confocal images in the sensory cortex and hippocampus of *Nampt*$^{f/f}$ and *Thy1-YFP-Nampt*$^{-/-}$ mice stained with MAP-2. Lower panels are high-resolution images of the boxed regions in the upper panels. e-f) Confocal maximal projection images (top). e'-f') Confocal single frame images (bottom). Notice that *Thy1-YFP-Nampt*$^{-/-}$ mice exhibited abnormal dendritic structures in the sensory cortex and hippocampal CA1 region and decreased MAP-2 immunoreactivity in the sensory cortex.

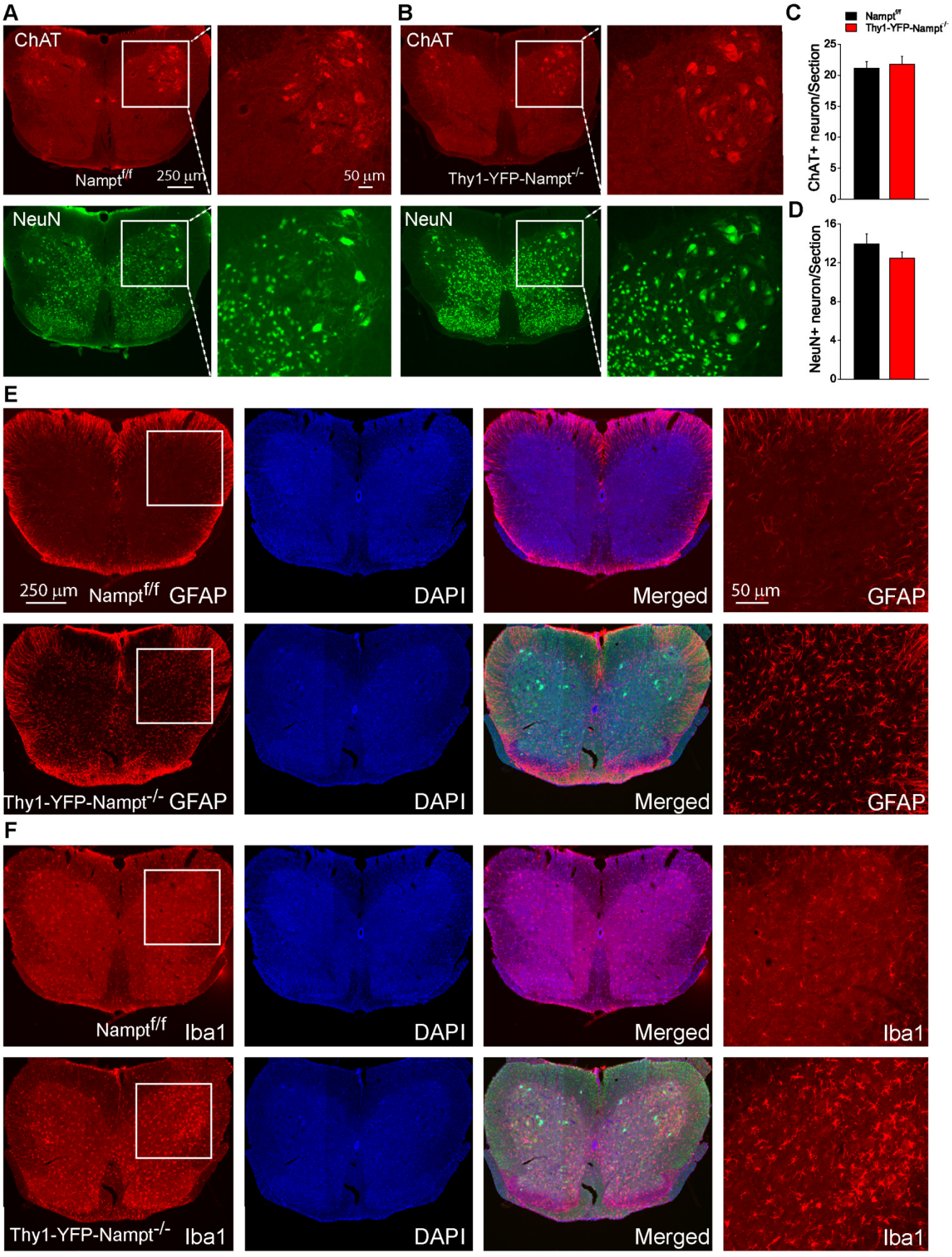
A
ChAT
Nampt f/f
250 μm
50 μm
B
ChAT
Thy1-YFP-Nampt -/-
NeuN
NeuN
C
Nampt f/f
Thy1-YFP-Nampt -/-
ChAT+ neuron/Section
0
5
10
15
20
25
D
NeuN+ neuron/Section
0
4
8
12
16
E
250 μm Nampt f/f GFAP
DAPI
Merged
50 μm
GFAP
Thy1-YFP-Nampt -/- GFAP
DAPI
Merged
GFAP
F
Nampt f/f Iba1
DAPI
Merged
Iba1
Thy1-YFP-Nampt -/- Iba1
DAPI
Merged
Iba1

Figure S4. Motor neuron death and reactive gliosis in the spinal cord of *Thy1-YFP-Nampt*$^{-/-}$ cKO mice (Related to Figure 3). (A-B) MNs of L3-5 spinal cord sections from *Nampt*$^{f/f}$ and *Thy1-YFP-Nampt*$^{-/-}$ mice stained with anti-ChAT and anti-NeuN antibodies. (C-D) Summary data of ChAT+ and NeuN+ neurons in the L3-5 spinal cord. Data were averaged from 4-6 sections from each mouse with a total of N=5 *Nampt*$^{f/f}$ mice and N=6 *Thy1-YFP-Nampt*$^{-/-}$ cKO mice. (E-F) Confocal images of GFAP (E) and Iba1 (F) staining in the L3-5 spinal cords. Right panels are high-resolution images of the boxed regions in the left panels. Error bars represent ±SEM.

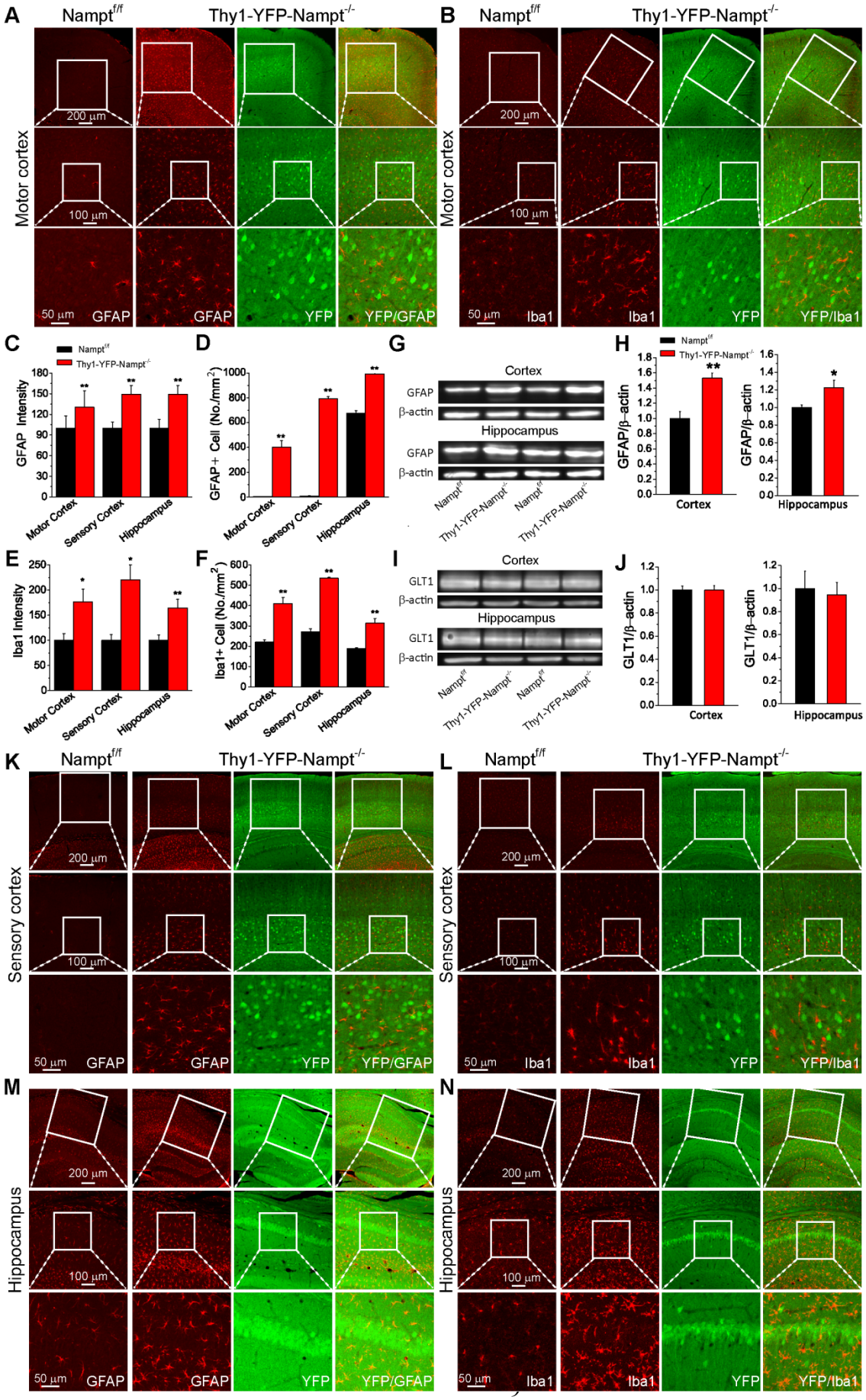
A
Nampt f/f
Thy1-YFP-Nampt -/-
Motor cortex
200 μm
100 μm
50 μm
GFAP
YFP
YFP/GFAP
B
Iba1
YFP/Iba1
C
GFAP Intensity
Motor Cortex
Sensory Cortex
Hippocampus
D
GFAP+ Cell (No./mm2)
E
Iba1 Intensity
F
Iba1+ Cell (No./mm2)
G
Cortex
Hippocampus
β-actin
H
GFAP/β-actin
I
GLT1
J
GLT1/β-actin
K
Sensory cortex
L
M
Hippocampus
N

Figure S5. *Thy1-YFP-Nampt*$^{-/-}$ cKO mice display global reactive gliosis in the brain (Related to Figure 3). (A-B) Representative maximal projection confocal images of GFAP (A) and Iba1 (B) staining in the motor cortices of *Nampt*$^{f/f}$ and *Thy1-YFP-Nampt*$^{-/-}$ mice. Lower panels are the high-resolution images of the boxed regions in the upper panels. (C and E) The mean GFAP (C) and Iba1 (E) fluorescence intensity in the motor cortices of *Nampt*$^{f/f}$ and *Thy1-YFP-Nampt*$^{-/-}$ mice within a standardized region of interest (598×1122 μm^2 in the cortical region of L4/5, and hippocampus CA1 region). (D and F) Average densities of GFAP+ (D) and Iba1+ (F) cells in the motor and sensory cortex and hippocampus of *Nampt*$^{f/f}$ and *Thy1-YFP-Nampt*$^{-/-}$ mice within the same standardized region of interest as in (C) and (E). N=5-6 mice for each genotype. (G-H) Western blot images and statistical analysis of GFAP expression in the cortex and hippocampus. Data were presented as the ratio of the GFAP/β-actin and normalized to the control mice. (I-J) Western blot images and statistical analysis of GLT1 expression in the cortex and hippocampus. In (H) and (J), N=4 mice for each genotype. *P < 0.05, **P < 0.01, t-test. (K-N) Representative maximal projection confocal images of GFAP (K-L) and Iba1 (M-N) staining in the sensory cortex and hippocampal CA1 region of *Nampt*$^{f/f}$ and *Thy1-YFP-Nampt*$^{-/-}$ cKO mice. Error bars represent ±SEM.

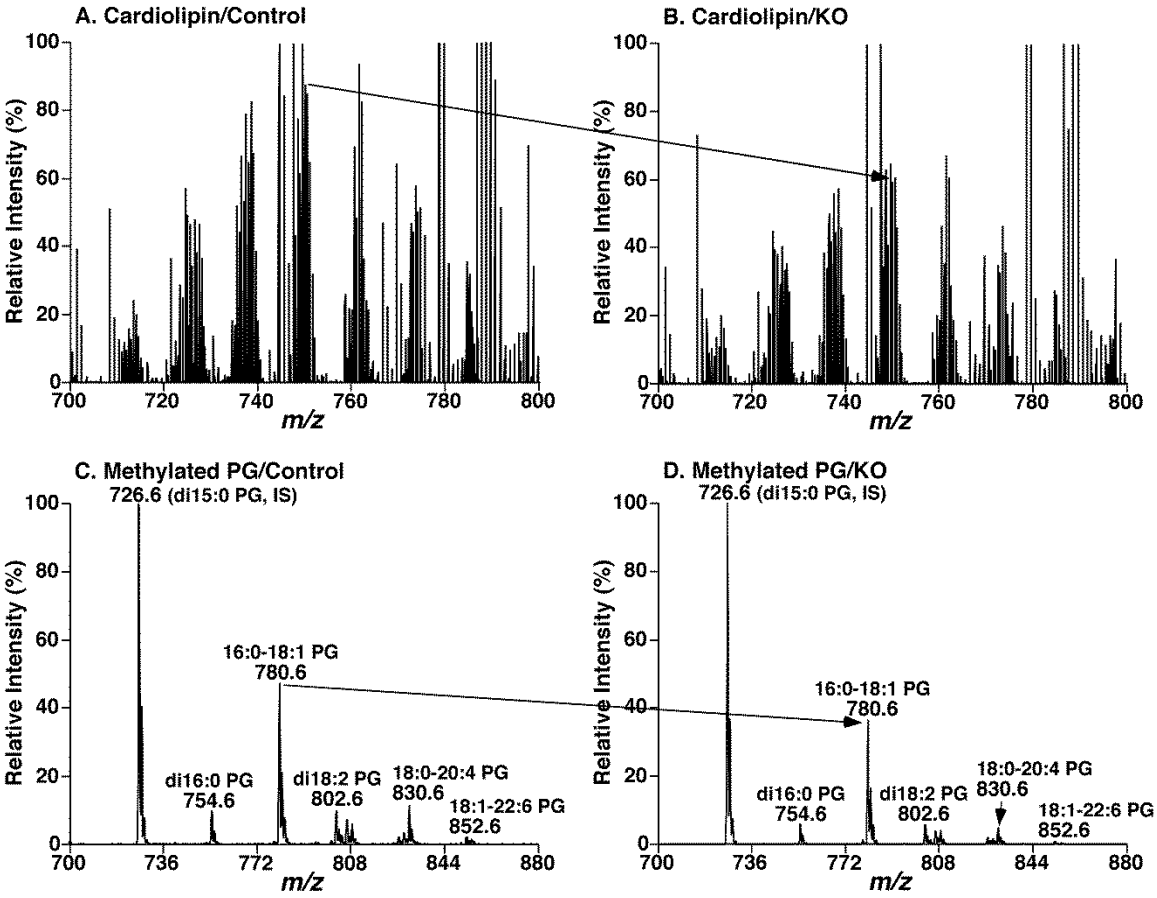

Figure S6. Mass spectral analysis of mitochondrial lipids (Related to Figure 4). Representative comparison of mass spectrometric analyses of cardiolipin (CL) and phosphatidylglycerol (PG) molecular species present in lipid extracts of cortices between control and *Thy1-YFP-Nampt*$^{-/-}$ cKO mice. Lipid extracts from brain tissue samples were prepared by a modified procedure of Bligh and Dyer extraction in the presence of internal standards (IS). Identification and quantification of individual lipid species were conducted by multi-dimensional mass spectrometry-based shotgun lipidomics as described in the method section. Mass spectra for analysis of CL (A-B) and PG (C-D) molecular species were displayed after normalization of the spectra to the spiked internal standards separately. The arrows indicate the reduction of CL and PG species, respectively.

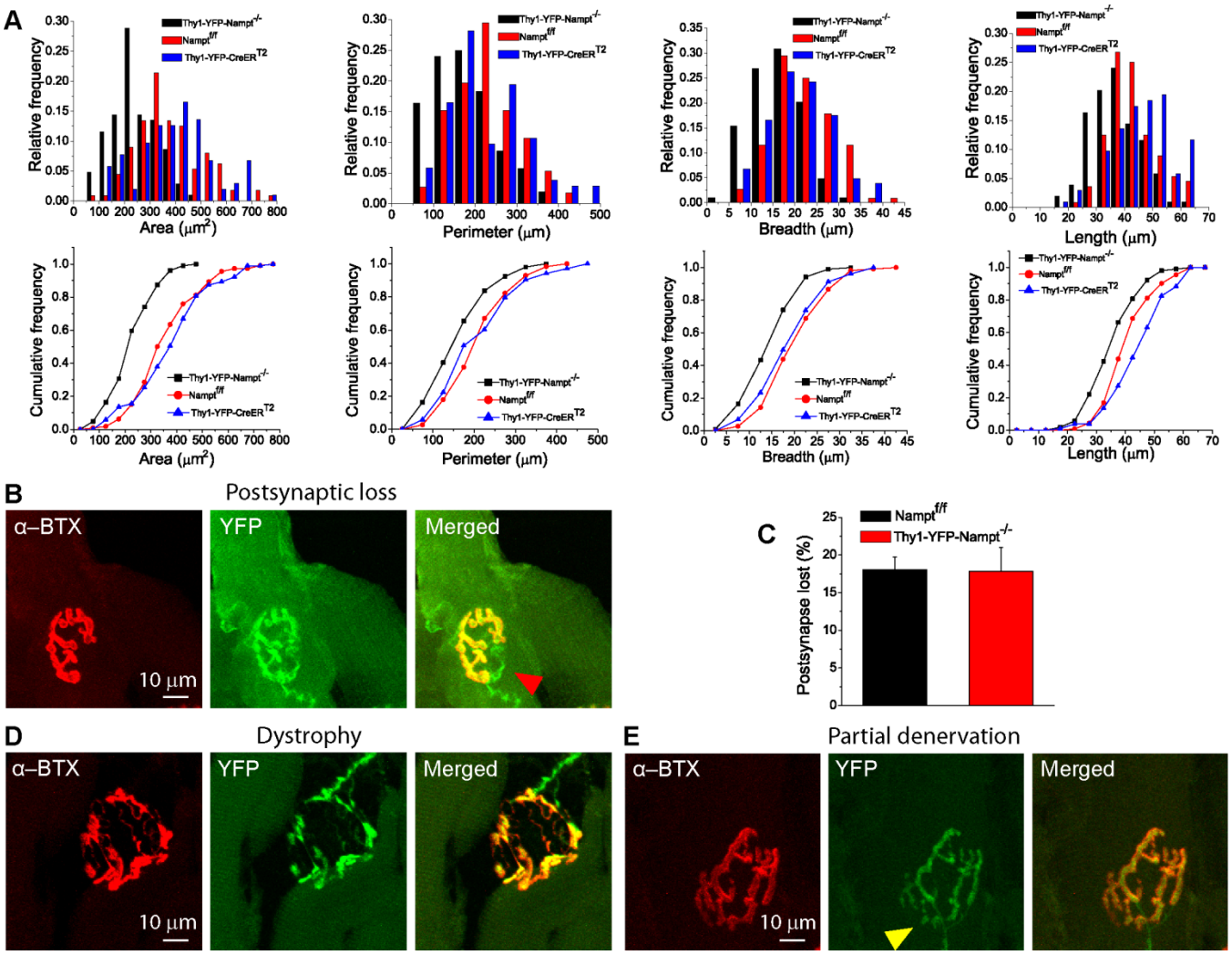

Figure S7. Postsynaptic loss and dystrophy of NMJs in *Thy1-YFP-Nampt*$^{-/-}$ mice (Related to Figure 5). (A) Frequency distributions (middle) and cumulative curves (bottom) of stained area, perimeter, breadth and length of individual NMJs. (B) Postsynaptic loss. Red arrowhead indicates a partial postsynaptic loss. (C) Statistical analyses of postsynaptic loss. N=3 mice for each genotype, n=506 and 144 NMJs for *Thy1-YFP-Nampt*$^{-/-}$ and *Thy1-YFP-CreER*^{T2} mice. (D) Confocal images of a dystrophic NMJ with a thin thread-like strand of pre- and/or post-synapse. Only 3 dystrophic NMJs out of 523 NMJs were found from three cKO mice, and no dystrophic NMJ was found in the control mice. (E) Confocal images of a NMJ with partial denervation. Error bars represent ±SEM.

Supplemental Experimental Procedures

Generation of *Nampt* cKO Mice

Mice were maintained on a 12 h light:12 h dark cycle (lights on 7 am-7 pm) in our AAALAC-accredited animal facility at the University of Missouri. To generate projection neuron-specific *Nampt* cKO mice, *Nampt$^{f/f}$* mice (Rongvaux et al., 2008) were crossed with *Thy1-CreER^{T2}-YFP* mice (Jackson laboratory) (Young et al., 2008) to obtain *Nampt$^{+/f}$:Thy1-CreER^{T2}-YFP* bitransgenic mice. *Nampt$^{+/f}$:Thy1-CreER^{T2}-YFP* mice were further bred with *Nampt$^{f/f}$* mice to obtain *Nampt$^{f/f}$:Thy1-CreER^{T2}-YFP* double homozygous transgenic mice. Genotypes were confirmed by PCR amplification of their DNA from tail snips (Li et al., 2015). *Nampt$^{+/f}$* and *Nampt$^{f/f}$* mice were used as controls for respective bitransgenic mice. To delete *Nampt* in *Nampt$^{+/f}$:Thy1-CreER^{T2}-YFP* or *Nampt$^{f/f}$:Thy1-CreER^{T2}-YFP* mice, TAM (200 mg/kg in sunflower seed oil, T5648, Sigma, MO) was administered for 5 consecutive days by oral gavage at the age of 8 weeks; sunflower seed oil was administered in Nampt$^{+/f}$ and *Nampt$^{f/f}$* mice for respective control experiments. The oral gavage administration of TAM for 5 consecutive days is a commonly used protocol in different studies including CNS and non-CNS systems. The recombination by Cre obtained by TAM oral gavage is more uniform, robust and rapid onset than IP injection (Park et al., 2008). We designate *Thy1-YFP-Nampt$^{+/-}$* and *Thy1-YFP-Nampt$^{-/-}$* for heterozygous and homozygous *Nampt* cKO mice. *Nampt$^{+/f}$* and *Nampt$^{f/f}$* mice were used as controls for respective bitransgenic mice. To study the effect of NMN on motor function, NMN (N2501, Sigma) was dissolved in saline (40 mg/ml) and administered through IP injection with a dose of 200 mg/kg. All procedures were performed according to the NIH Guide for the Care and Use of Laboratory Animals and were approved by the University of Missouri Animal Care Quality Assurance Committee.

General Conditional Score

In order to assess the general condition of knockout mice, the mice were visually inspected daily for the assessment of general morphological and motor abnormalities including the appearance of hunched and piloerection posture and the onset of hindlimb clasping when lifted by the tail and waddling walk gaits. We set up a 5-points (1-5) behavioral scoring system based on a scoring system used in an ALS model (Knippenberg et al., 2010):

5 points: normal and healthy without any symptoms of paralysis;

4 points: slight signs of destabilized gait and paralysis of the hindlimbs;

3 points: obvious signs of destabilized gait and paralysis of the hindlimbs; when holding the tail, hindlimbs sometimes clasped;

2 points: fully developed paralysis of the hindlimbs, animals only crawl on the forelimbs; when holding the tail, hindlimbs often clasped;

1 point: fully developed paralysis of the hindlimbs and animals predominantly lie on the side; when holding the tail, hindlimbs always clasped.

The general condition was assessed by two trained observers respectively, and the average of these two scores was used as the general condition score. When reaching a score of 2 points, full hindlimb paralyzed mice were given macerated food daily on a shallow plastic plate next to water for easy access.

Analysis of Muscle Atrophy, Disease Progress and End-Stage

The mice were visually inspected daily for the assessment of general morphological and motor abnormalities including the appearance of hunched and piloerection posture and the onset of hindlimbs clasping when lifted by the tail and waddling walk gaits. The time of disease end-stage was defined when the paralyzed mice were unable to right themselves within 20 s when placed on their side or found in lateral recumbency (Boillee et al., 2006;Kang et al., 2013), at which point mice were euthanized.

Behavioral Tests

Behavior tests below were performed between 8:00 am-12:00 pm. All the animals were taken out from animal room in their home cages to the behavior test room and habituated for at least 30 min starting at 7:30 am. For each type of behavior test, the pre-training was conducted twice before pre-recording of the behavior test, which was taken 1 or 2 days before TAM administration. TAM was administrated with oral gavage for 5 consecutive days (day 1 to day 5). Day 6 was the first day post TAM administration (PTA). Both of the pre-recording days were defined as day 0 in our experiments. We conducted open field, rotarod tests on day 6, 10, 14, 18, 20, 22, 24 and 26, while cylinder test, pole test and hanging wire test (in this order) were completed on day 7, 11, 15, 19, 21, 23, 25 and 27, since day 18 was the average disease onset time point to show slight symptoms in Thy1-YFP-Nampt$^{-/-}$ mice. Mice were given an interval of at least 30 min for recovery in their home cages between two different behavior tests. All apparatuses were cleaned with 20% ethanol and dried between tests to avoid olfactory effects.

The cylinder test. The cylinder test was designed to evaluate the severity of paralysis of the hindlimbs (Schaar et al., 2010). The mouse was placed in a transparent cylinder 9 cm in diameter and 12 cm high. Use of forelimbs to touch the wall was recorded. The number of times the mouse stood up on hindlimbs and used forelimbs to touch the wall was recorded over a period of 2 min after 30 s calm-down time in the cylinder.

The hanging wire test. We performed the hanging wire test to assess grip strength of forelimbs and body balance as previously described (Li et al., 2014;Li et al., 2015). The mouse was pre-trained twice. Mice utilized forelimbs to hang their body weight on a wire stretched between two posts with an interval of 50 cm at the same heights of 60 cm above the ground. The time until the mouse dropped off the wire was recorded. A time of zero was assigned if the mouse dropped off immediately while 120 s was the maximum period. Two trials were performed for each mouse at each time point.

The pole test. The pole test is a simple test, with minimal equipment, to evaluate bradykinesia and motor coordination (Li et al., 2014;Li et al., 2015). The mouse was first placed upward on the top of a metal pole (with a diameter of 10 mm and a height of 50 cm) covered with adhesive tape to prevent the mouse from sliding or falling down. The time to turn around and descend down to reach the ground was recorded. Both the knockout mice and their corresponding control mice can learn the pole test by two-day pre-training and then can be tested repeatedly. The pre-training included two steps: to place the mouse facing downward on the top of the pole and let it descend down to touch the ground for 5 times, and then to place the mouse facing upward and let it turn around and start descending procedure itself. If the mouse tended to hold at the top or paused during the turn or downward movement, then the trial was excluded and repeated after an interval of at least 5 min.

Open field test. The open field test is widely used to evaluate motor function and normal exploratory locomotion (general locomotor activity) and thigmotaxis (Brooks and Dunnett, 2009;O'Leary et al., 2016;Tatem et al., 2014). After at least 30 min habituation in the open field test room, the mouse was placed in the center of the open field apparatus consists of a clear, open Plexiglas box (46.6 cm×38.5 cm×25.6 cm) with an overhead camera to record horizontal movements over a 20-min period by ANY-maze software (Stoelting, IL). Parameters included total travel distance, total immobile time, the ratio of corner travel distance to total travel distance and time spent in the corner were also quantified by ANY-maze software. The sensitivity for the detection of immobile was set as 65 % of the body area. The animal needed to remain immobile for 5 s before it was considered to be immobile.

Rotarod test. The rotarod test can evaluate motor function, coordination and balance in mice (Brooks and Dunnett, 2009). It was conducted using a five-station accelerating rotarod apparatus having a black striated rod with a diameter of 3.2 cm, a falling height of 16.5 cm and a lane width of 5.7 cm (ENV-577M, Med Associates, Inc., VT). Two-day pre-training was performed to allow mice to learn to walk on the accelerating rod. Mice were placed on the rod and allowed to move freely as the rotation increased from 4 to 40 rpm over an 180 s period (Inoue et al., 2014). The time was recorded when the mouse fell from the rod or when the mouse had ridden the rotating rod for two revolutions without regaining control. If mice dropped within 180 s, a second chance was given to them after 20 min recovery.

Grip strength tests. The grip strength tests were performed to assess the neuromuscular strength of forelimbs and all four limbs respectively (Brooks and Dunnett, 2009). Grip strength was measured by a digital grip strength meter (Mark-10 Corporation, Copiague, NY). The apparatus included a triangle metal pulling bar or a triangular grid attached to a force transducer. The pulling bar is used for forelimb strength measurement and a grid used for combined strength of forelimbs and hindlimbs (four limbs). The mouse was gripped by the base of the tail and gently lowered to allow the forelimbs or both forelimbs and hindlimbs to grab the pulling bar or triangular grid. The mouse's body remained parallel with the grid when it was gently and steadily pulled back by its tail and peak force was recorded from the reading when the mouse released the pulling bar or grid. Each mouse was tested over the course of five trials with an inter-trial interval at least 30 s respectively for its forelimbs as well as all four limb grip strength. The largest three values of the five were chosen, and the average value was taken for statistical analysis.

Body Weight and Abdominal Temperature Measurements

Mice's body weight and temperature were recorded daily, starting at 8 weeks of age, two days before TAM administration. Mice were placed in a plastic box with lid and weighed by a digital balance. Abdominal temperature was measured by an infrared thermometer with an accuracy of 0.1 °C (ThermoWorks, UT). The measurement was performed between 7:00-7:30 am, when mice were placed in the behavior test room for habituation to avoid diurnal variations.

Weight Measurements of Organs

Fresh brain, heart, lung, liver, kidney, gastrocnemius and soleus muscles were collected from *Thy1-YFP-Nampt*$^{-/-}$, *Thy1-YFP-Nampt*$^{+/-}$ and *Nampt*$^{f/f}$ mice immediately after euthanasia. The weights of these tissues were measured by a digital balance.

Isolation and Characterization of NMJs

Mice were euthanized, and the semitendinosus muscles were freshly isolated from *Thy1-YFP-Nampt*$^{-/-}$ (Polo-Parada et al., 2004), *Nampt*$^{f/f}$ and *Thy1-YFP-CreER*^{T2} mice 3 weeks after TAM administration. The semitendinosus muscle is innervated by fast motor neurons and primarily consists of fast-twitch muscle fibers with rapid contractions in a short time and is responsible for flexion of knee and extension of hip (Kariya et al., 2008). We chose the semitendinosus muscle for detailed analysis of NMJs because of its unique features such as large size, quasi-homogeneous fiber type and flat morphology; more importantly, it contains plentiful stable NMJs in a fairly large region compared with other hindlimb muscles such as gastrocnemius and soleus, and therefore has been widely used to examine the NMJ alterations (Polo-Parada et al., 2004). The entire muscles were incubated with 5 μg/mL (1:1,000 dilution) Alexa Fluor 594 conjugated α-Bungarotoxin (α-BTX-Alexa 594) (B13423, Thermo Fisher Scientific) in saline for 30 min. After 10-min washing with 0.01 M PBS for three times, the muscles were post-fixed in 4% paraformaldehyde (PFA) in PBS overnight. In order to assess the pre-synaptic

axon in *Nampt*$^{f/f}$ mice, the whole mount semitendinosus muscles were blocked with 10% donkey serum (Jackson ImmunoResearch, PA) for 1 h at room temperature, and were stained with rabbit anti-neurofilament 200 (1:400, N4142, Sigma) for 48 h followed by 4-h incubation with Donkey anti-rabbit-IgG-Alexa-647 second antibody (1:300, A-31573, Life Technologies). Stained muscles were embedded in Tissue-Tek O. C. T. Compound and longitudinal sections of 50 μm thick were cut using a cryostat. Stained sections were sealed with Permount (UN1294, Fisher Scientific) and imaged with an Olympus FV1000 confocal microscope using a 40x objective.

The NMJ architecture characterization was based on the definitions given by Valdez et al. (Valdez et al., 2010). Only NMJs with a pretzel-shaped morphology that stained positive for α-BTX binding to the acetylcholine receptor (AChR) were quantified on three nonadjacent sections at least 100 μm apart per mouse. More than 100 NMJs from 3 mice for each group were captured throughout all the regions of semitendinosus muscle slices. Maximum intensity projections of stacking images (40×, 1024 pixels by 1024 pixels) obtained by Olympus FV1000 confocal microscope were created to analyze NMJs with off-line MetaMorph software (Molecular Devices, CA). For the size analysis, we set up four parameters, *i.e*., the stained area, the perimeter, the length and the breadth, of a single postsynaptic end-plate. Neuromuscular junctions were defined as innervated when axon terminals with fluorescently labeled AChRs were colocalized. We defined nine different types of abnormal or irregular morphology of NMJs as follows (Seijffers et al., 2014;Valdez et al., 2010;Valdez et al., 2012): 1) Fragmentation: an AChR cluster was broken into several segments that were not connected with each other. 2) Faint AChRs: the postsynapse in part or in whole was weakly labeled with α-BTX resulting from AChR density decrease compared with others in the same confocal plane. 3) Postsynaptic loss: the presynapse, represented by YFP, was not fully occupied by AChR clusters. 4) Partial or complete denervation: nerve terminals retracted completely or partially in postsynaptic sites, so part of or all region of the motor end-plate was not overlapped by YFP-labeled nerve terminal. 5) Non-innervation: the AChR-rich postsynaptic site was not aligned with an axon terminal. 6) Multi-innervation: one post-synapse was innervated by more than one pre-synaptic terminal. 7) Swollen axon: distension or dilation on the presynaptic axon within 10–50 μm proximally to the postsynapse. 8) Sprouting (NMJ sprouts): the presynaptic axon extended beyond the neuromuscular junction site, *i.e.*, nerve terminals that do not terminate within an AChR cluster, and then sometimes made contact with another AChR cluster. 9) Dystrophy: the pre- and/or postsynapse consisted of filamentous or thin thread-like strand.

Transcardial Perfusion, Nissl Staining and Immunohistochemistry

The procedures were similar to our previous studies (Li et al., 2014;Li et al., 2013;Wang et al., 2016;Zhang et al., 2010). Adult mice were transcardially perfused with 0.01 M phosphate buffer saline (PBS), followed by ice-cold 4% paraformaldehyde (PFA) in 0.01 M PBS (pH 7.4) under deep anesthesia. After perfusion, the brains and spinal cords were removed and post-fixed in 4 % PFA in PBS at 4 °C overnight. It was then dehydrated in 30 % sucrose in PBS for 2-3 days. Brain coronal sections and L3-5 transverse spinal cord sections (30 μm) were cut using a cryostat and collected serially on pre-gelatin coated glass slides or in a 48-well plate with cryoprotectant and stored at -20 °C until use. For Nissl staining, brain slices were stained with 0.25 % cresyl violet. For immunostaining, brain or muscle slices were washed with PBS three times carefully and were then blocked with 10 % serum in 0.3 % Triton X-100 in PBS at room temperature for 1 h. Brain slices were then incubated with primary antibody: rabbit anti-NAMPT polyclonal antibody (1:300, A300-372A, Bethyl Laboratories), mouse anti-NAMPT polyclonal antibody (1:600, P4D5AT, Enzo Biochem), mouse anti-NeuN polyclonal antibody (1:300, MAB377, Millipore), mouse anti-S100β monoclonal antibody (1:300, S2532, Sigma), mouse anti-MAP2 monoclonal antibody (1:300, MAB3418, Millipore), rabbit anti-ionized calcium-binding adaptor molecule 1 (Iba1) antibody (1:500, #019-19741, Wako Chemicals), rabbit anti-glial

fibrillary acidic protein (GFAP) polyclonal antibody (1:300, G9269, Sigma), mouse anti-slow skeletal myosin heavy chain (1:500, ab11083, Abcam) in 1 % serum, 0.3 % Triton X-100 in PBS at 4 °C overnight. The brain slices were then washed three times each for 5 min with PBS and incubated with fluorescently labeled secondary antibody: Alexa 568-conjugated donkey anti-mouse IgG (1:200, A10037, Life Technologies) or Alexa 647-conjufaetd donkey anti-rabbit IgG (1:200, A31573, Life Technologies) in 1 % serum, 0.3 % Triton X-100 in PBS for 4 h in the dark at room temperature. The nuclei were stained with DAPI (P36931, Life Technologies). The samples were subjected to fluorescence detection using an Olympus confocal microscope and analyzed by MetaMorph software (Molecular Devices) under an experimenter blind to experimental conditions. The same settings were kept for the same kind of staining. For the quantifications and morphological analyses of neuron degeneration, the average fluorescence intensity of neuronal markers NeuN and MAP-2, astrocytic marker GFAP and microglia marker Iba1 were measured in the motor cortex, sensory cortex and hippocampus of NAMPT cKO and control mice. Moreover, the densities of GFAP and Iba1 positive cells (No./mm^2) in the same region were also calculated. The data were collected from 2 slices of each mouse and 5-6 mice per genotype for each kind of staining.

Mitochondrial Fraction Isolation

Mitochondrial fractions were isolated from brain cortical tissues of mice using the commercial mitochondrial isolation kit (Thermo Fisher Scientific, 89874). All manipulations were performed according to the manufacturer's instruction. Briefly, brain tissue was cut into small pieces and washed extensively by PBS before isolation. The sample was homogenized using a dounce homogenizer. The lysate was centrifuged for 10 min at 1000 g at 4 °C. The pellet which contains nuclei and cell debris was discarded. The supernatant was centrifuged at 3,000 g for 15 min at 4 °C. The pellet contained the isolated mitochondria.

FM1-43 Labeling of Synaptic Vesicles and Electrophysiological Recordings of NMJs

Synaptic vesicle labeling and standard electrophysiological recordings were described previously (Maeno-Hikichi et al., 2011;Polo-Parada et al., 2005). Semitendinosus muscles were isolated and placed in Tyrode's solution (137 mM NaCl, 5 mM KCl, 12 mM $NaHCO_3$, 1 mM $MgCl_2$, 2 mM $CaCl_2$, 0.2 mM Na_2HPO_4 and 10 mM glucose) containing 80 μM FM1-43 (T35356, Life Technologies) and 1 μg/ml α-BTX-Alexa 488 (B13422, Life Technologies) and oxygenated with 95% oxygen and 5% CO_2. Synaptic vesicles were labeled with FM1-43 by stimulating the nerve fiber with 10 Hz frequency for 10 min. The muscles were then fixed with 4% PFA for 30 min and subsequently sectioned with a thickness of 40 μm using a cryostat for confocal imaging of α-BTX and FM1-43. For electrical recordings, sharp glass electrodes (20–40 M) were filled with 3 M KCl and single muscle fibers were impaled near the motor end-plate in Tyrode's solution. Evoked end-plate Potentials (eEPPs) and spontaneous miniature EPPs (mEPPs) were recorded via a BA-1S amplifier (npi electronic GmbH, Germany) using Axoscope software (Axon Instruments, CA). The nerves were sucked into tight polyethylene-stimulating electrodes and stimulated with a Grass S88 stimulator thorough a PSIU6B isolation unit (Grass Instruments, MA). The muscle contraction was prevented by pre-incubation of 100 nM μ-conotoxin to block voltage gated sodium channels in muscle.

Western Blotting

Western blotting was used to analyze NAMPT and other protein expressions in the cortex, hippocampus, spinal cord and non-CNS organs including muscle, heart, liver and kidney following the protocol described in our previous studies (Li et al., 2013;Li et al., 2015;Wang et al., 2014;Wang et al., 2016;Zhang et al., 2010). Protein was extracted from fresh tissues, and then dissolved in lysis buffer mixed with protease inhibitor (Pierce Biotechnology, Rockford, IL) and phosphatase inhibitor cocktails

(Sigma). The homogenized tissue was centrifuged at 13,500 g for 30 min at 4 °C, and the total cell lysate was kept in the supernatant. We used the bicinchoninic acid (BCA) protein assay kit (Pierce Biotechnology) to test the protein concentration of the cell lysate. Equivalent amounts of protein from each sample were diluted with lysis buffer and boiled for 5 min. Samples were subjected to electrophoresis in 10% SDS-polyacrylamide gels at 100 mV for 100-110 min, and transferred to polyvinylidene fluoride membranes at 100 mV for 1 h. The membranes were blocked for 1 h by 5% (w/v) nonfat dry milk powder in Tris-buffered saline containing 0.1% (v/v) Tween-20 (TBS-T). The membranes were then incubated overnight at 4 °C with mouse monoclonal anti-NAMPT (1:1000, ALX-804-922-C100, Enzo Life Sciences), rabbit polyclonal anti-NAMPT antibody (1:1000, A300-372A, Bethyl Laboratories), mouse anti-excitatory amino transporter 2 antibody (GLT-1, 1:1000, MAB2262, Millipore, CA), mouse monoclonal anti-GFAP (1:2500, G3893, Sigma), rabbit monoclonal anti-neuronal nuclei antibody (NeuN, 1:1000, MABN140, Millipore), rabbit anti-Sirt1 antibody (DAM1780373, 1:1000, Millipore), rabbit anti-Sirt3 antibody (1:1000, ab86671, Abcam), goat anti-NMNAT3 antibody (1:1000, ab121030, Abcam), mouse anti-p53 antibody (1:500, MABE283, Millipore), rabbit anti-mitofusin-2 antibody (1:1000, #9482, Cell Signaling), rabbit anti-Drp1 antibody (1:1000, ABT155, Millipore), rabbit anti-p-Drp1 antibody (1:1000, #3455, Cell Signaling), rabbit anti-Acetylated lysine antibody (1:1000, #9441, Cell Signaling), rabbit anti-TOM20 antibody (1:1000, sc-11415, Santa Cruz Biotechnology), rabbit anti-LC3B antibody (1;1000, NB600-1384, Novus), mouse anti-PSD95 antibody (1:1000, NB300-556, Novus), mouse anti-synaptophysin antibody (1:1000, S5768, Sigma), rabbit anti-NMDAR2B antibody (1:1000, NB300-106, Novus), rabbit anti-PAR antibody (1:1000, #551813, BD Pharmingen), rabbit anti-caspase 9 antibody (1:1000, #9504, Cell Signaling), rabbit anti-PGC-1α polyclonal antibody (1:500, sc-13067, Santa Cruz), rabbit anti-NRF-1 polyclonal antibody (1:500, sc-33771, Santa Cruz) in 5% (w/v) non-fat dry milk. After washing with TBS-T, the membranes were incubated with appropriate second antibodies HRP (horseradish peroxidase)-conjugated rabbit anti-mouse IgG (1:2500, A9044, Sigma), HRP-conjugated goat anti-rabbit IgG (1:2500, A0545, Sigma) or peroxidase AffiniPure bovine anti-goat IgG (1:2500, 805-035-180, Jackson ImmunoResearch), in 5% (w/v) non-fat dry milk for one hour at room temperature. Monoclonal mouse anti-β-actin antibody (1:1000, cs-47778, Santa Cruz) and Cox IV (1:1000, sc58348, Santa Cruz) were used as a control of equal loading for the total protein in whole cell lysate and mitochondrial fractions. The membranes were exposed to Pierce ECL detection reagents (Pierce Biotechnology) and scanned with the Fuji LAS 3000 densitometer to visualize protein bands. Precision Plus Protein™ Dual Color Standards (#1610374, Bio-Rad, CA) was used as the marker to evaluate the molecular size of protein bands.

NAD^+ and NADH Measurement in Brain Tissue

The contents of NAD^+ and NADH were measured using a commercially available assay kit (E2ND-100, Bioassay Systems, CA) (Bi et al., 2012). Freshly harvested cortical tissues (~5 mg) were placed into a 1.5 mL tube with 100 μL NAD^+ or NADH extraction buffer and homogenized on ice. The extracts were heated at 60 °C for 5 min, and then 20 μL assay buffer and 100 μL of the opposite extraction buffer were added to neutralize the extracts. The samples were briefly mixed and spun down at 14,000 rpm for 5 min. The supernatant was used for NAD^+ or NADH enzymatic assay. The total NAD^+ and NADH level were expressed as pmol/mg tissue.

Motor Neuron Counting

ChAT+ MNs and large NeuN+ α-MNs of L3-5 spinal cords in ventral horn were manually counted based on confocal images using Metamorph software (Friese et al., 2009;Wong and Martin, 2010). The number of MNs per section of the spinal cord was averaged from 5-6 sections, and used as a single value per mouse. The mean number per section for each genotype was the average value from 5-6 mice.

Type I Slow-Twitch Muscle Fiber Counting and Cross Section Area (CSA) Analysis

The cross-section slices of semitendinosus muscle with 10 μm thick were stained with anti-slow skeletal myosin heavy chain to identify type I slow-twitch muscle fibers. The number of muscle fibers with positive staining (*i.e*., with bright fluorescent signal within the fibers) and the total number of muscle fibers were counted, and CSAs of muscle fibers were analyzed using Metamorph software. The ratios of the number of type I muscle fiber to the total number of muscle fiber and CSAs were compared between *Nampt*$^{f/f}$ and *Thy1-YFP-CreER*^{T2} mice.

Shotgun Lipidomic Analysis of Lipids from Mouse Tissues

Shotgun lipidomics of lipid extracts of mouse brain cortices was performed as described previously (Yang et al., 2009;Yang and Han, 2011). Briefly, lipids were extracted by a modified procedure of Bligh and Dyer as previously described A triple-quadrupole mass spectrometer equipped with a Nanomate device and Xcalibur system was utilized to analyze lipids. All tandem mass spectrometry analyses were automatically acquired by a customized sequence operated under Xcalibur software as described (Yang et al., 2009). Internal standards were added to each tissue sample prior to extraction based on total protein content of the sample for quantification of individual molecular species of lipid classes. Protein content was determined using a bicinchoninic acid protein assay kit (Thermo Scientific, Rockford, IL). Quantification of lipid species in comparison to the corresponding internal standards was conducted following the principles of shotgun lipidomics with different MS/MS scans specific to each class of lipids as previously described (Yang and Han, 2011).

Mitochondrial Enzymatic V_{max} Activity Assays of Brain Tissue

Cortical tissues (~50 mg for each sample) were cut into small pieces and homogenized with a Dounce homogenizer in 1 ml of 20 mM PBS containing protease and phosphatase inhibitors. The homogenate was diluted to four fold with 20 mM PBS and used to determine the enzymatic activities of Complex I (or NADH dehydrogenase), Complex IV (or cytochrome oxidase) and citrate synthase (CS) using an Infinite M200 plate reader (Tecan Group Ltd., Switzerland) as described previously (Ghosh et al., 2007). The protein concentration of homogenate was determined using the DC (detergent compatible) protein assay (5000116, Bio-Rad Laboratories, CA). The maximal reaction speed (V_{max}) normalized to the amount of protein was used to characterize the activity of each enzyme. For the Complex I V_{max} assay, diluted homogenate was first subjected to three freeze and thaw cycles. Next, 15 mM Coenzyme Q1 was added into a cuvette containing 150 μM NADH and 40 μl diluted homogenate. The decrease in NADH absorbance at 340 nm was monitored for 2 min for estimate V_{max}. To measure the Complex I induced NADH oxidation, 10 nM Cox I inhibitor rotenone was added and the post-rotenone rate was subtracted from the pre-rotenone rate to yield the rotenone-sensitive NADH oxidation V_{max}. For the Complex IV V_{max} assay, 25 μM reduced cytochrome c was added into the cuvette containing 20 mM PBS, 5 μl diluted homogenate and 0.2 mg/ml dodecyl maltoside. The total volume of mixture was 1 ml. The oxidation of the reduced cytochrome c was monitored for 2 min at 550 nm and the pseudo first-order rate constant was calculated as V_{max}. For the CS V_{max} assay, the substrates of CS, 100 μM oxaloacetate and 50 μM acetyl CoA were added into the cuvette containing 100 mM Tris-HCl (pH 8.0), 5 μl homogenate and 100 μM 5,5'-dithiobis-(2-nitrobenzoic acid) (DTNB) (1 ml total volume) and then the formation of 5-mercapto-2-nitrobenzoic acid was monitored for 2 min at 412 nm.

Mitochondrial Respiration Flux Assay of SH-SY5Y Cells

Undifferentiated human neuronal SH-SY5Y cells were cultured in high glucose Dulbecco's modified Eagle medium (DMEM) supplemented with 10 % fetal bovine serum (FBS) and 1 % penicillin-streptomycin in a 37 °C, 5 % CO_2 incubator. To test the effect of NAMPT on respiration, SH-SY5Y

cells were plated in 6-well plates and XF24 cell culture microplates (Seahorse Bioscience, MA) and transfected with scrambled and *Nampt*-targeting siRNA (GE Healthcare Dharmacon, Inc., IL) one day later using lipofectamine 2000. Forty eight hours after transfection, cells cultured in 6-well plates were harvested for Western blot analysis to confirm the reduction of NAMPT in the cells transfected by *Nampt*-targeting siRNA. For oxygen consumption rate (OCR) measurement, the individual wells in XF microplate were washed and replaced by serum-free, pyruvate-free, and buffer-free DMEM supplemented with 25 mM glucose. The plate was incubated in a 37 °C, non-CO_2 incubator for 1 h and then transferred to the microplate stage of a Seahorse XF24 extracellular flux analyzer (Aligent Tech., CA) for OCR measurement following the procedure described previously and in the Seahorse Mitochondrial Stress Test kit (Wilkins et al., 2016). Initial OCR measurements were taken using a 3 min mixing, 2 min wait and 3 min read cycling protocol. Three separate readings were taken to ensure stability. Next, oligomycin was added to each well (2 μM final concentration) and three separate OCR readings were taken, followed by an injection of carbonyl cyanide-p-trifluoromethoxyphenylhydrazone (FCCP) in each well (0.3 μM final concentration) and three separate OCR readings were taken. Finally, a mixture of rotenone and antimycin A was injected into each well (1 μM final concentration of each inhibitor) and three separate OCR readings were taken. For each well, the area under curve (AUC) from the pre-oligomycin period was used to represent the baseline OCR for the well. The post-rotenone/antimycin A OCR for each well was subtracted from the baseline OCR to provide a true mitochondrial respiration rate. To calculate the leak rate the post-rotenone/antimycin A OCR was subtracted from the post-oligomycin OCR for each well. The ATP rate was calculated by subtracting the leak for each well from the baseline OCR. The post-rotenone/antimycin A OCR was subtracted from the post-FCCP OCR to determine the FCCP-induced maximum respiration rate. Data were normalized by the total amount of protein, which was measured using a DC assay.

Analysis of Mitochondrial DNA (mtDNA) Relative to Nuclear DNA (nucDNA)

Real time PCR (RT-PCR) was used to quantify the relative content of mtDNA to nucDNA, *i.e.*, mtDNA/nucDNA. The total DNA of cortical tissue was extracted and purified using the genomic DNA extraction kit (69504, Qiagen Sciences, Inc., CA). We used 12S rRNA and 18S rRNA genes specific primers for the mtDNA and nucDNA quantifications. The primers used for mtDNA were (Bi et al., 2012): 5'-ATTTCGTGCCAGCCACCGCGG-3' (forward); 5'-GGCTACACCTTGACCTAACGT-3' (reverse). The primers for nucDNA were: 5'-GGAATAATGGAATAGGACCGCG-3' (forward); 5'-GGACATCTAAGGGCATCACAG-3' (reverse). One hundred ng of total DNA was assessed by RT-PCR using a 7900HT Fast Real-Time PCR System (Applied Biosystems). The reaction was performed in triplicate in a final volume of 20 μl with 2×SYBR green PCR master mixture (B21203, Biomake.com) and 0.15 μM of the reverse and forward primers. PCR reaction was performed at 95°C for 2 min, then 30 cycles at 95 °C for 20 s, 58 °C for 20 s and 72 °C for 30 s, and followed by 72 °C for 7 min for the final extension. PCR products are 655 bp for nucDNA and 464 bp for mtDNA. Both mtDNA and nucDNA Ct values were obtained from RT-PCR software, and the Ct values for each mouse were averaged from triplicate reactions for each sample. mtDNA copies relative per diploid nucDNA (mtDNA/nucDNA) for the control and knockout mice were calculated and averaged (N=5 mice for each genotype) using the following equation (Rooney et al., 2015): ΔCt= Ct (nucDNA)-Ct (mtDNA) and mtDNA/nucDNA=$2\times2^{\Delta Ct}$.

Human ALS Samples and NAMPT Analysis

Human lumbar spinal cord frozen tissues (10 ALS patients and 10 age-matched controls) were obtained from the NICHD Brain and Tissue Bank for Developmental Disorders at the University of Maryland, Baltimore, MD with contract HHSN275200900011C and Ref. No. N01-HD-9-0011. For Western blot

analysis of iNAMPT and eNAMPT, rabbit anti-NAMPT antibody (1:5000) and rabbit anti-β-actin antibody were used.

Supplemental References

Bi,J., Li,H., Ye,S.Q., and Ding,S. (2012). Pre-B-cell colony-enhancing factor exerts a neuronal protection through its enzymatic activity and the reduction of mitochondrial dysfunction in in vitro ischemic models. Journal of Neurochemistry *120*, 334-346.

Boillee,S., Yamanaka,K., Lobsiger,C.S., Copeland,N.G., Jenkins,N.A., Kassiotis,G., Kollias,G., and Cleveland,D.W. (2006). Onset and progression in inherited ALS determined by motor neurons and microglia. Science *312*, 1389-92.

Brooks,S.P., and Dunnett,S.B. (2009). Tests to assess motor phenotype in mice: a user's guide. Nat Rev Neurosci *10*, 519-529.

Friese,A., Kaltschmidt,J.A., Ladle,D.R., Sigrist,M., Jessell,T.M., and Arber,S. (2009). Gamma and alpha motor neurons distinguished by expression of transcription factor Err3. PNAS *106*, 13588-13593.

Ghosh,S., Patel,N., Rahn,D., McAllister,J., Sadeghi,S., Horwitz,G., Berry,D., Wang,K.X., and Swerdlow,R.H. (2007). The Thiazolidinedione Pioglitazone Alters Mitochondrial Function in Human Neuron-Like Cells. Molecular Pharmacology *71*, 1695-1702.

Inoue,T., Hoshina,N., Nakazawa,T., Kiyama,Y., Kobayashi,S., Abe,T., Yamamoto,T., Manabe,T., and Yamamoto,T. (2014). LMTK3 Deficiency Causes Pronounced Locomotor Hyperactivity and Impairs Endocytic Trafficking. The Journal of Neuroscience *34*, 5927-5937.

Kang,S.H., Li,Y., Fukaya,M., Lorenzini,I., Cleveland,D.W., Ostrow,L.W., Rothstein,J.D., and Bergles,D.E. (2013). Degeneration and impaired regeneration of gray matter oligodendrocytes in amyotrophic lateral sclerosis. Nat Neurosci *16*, 571-579.

Kariya,S., Park,G.H., Maeno-Hikichi,Y., Leykekhman,O., Lutz,C., Arkovitz,M.S., Landmesser,L.T., and Monani,U.R. (2008). Reduced SMN protein impairs maturation of the neuromuscular junctions in mouse models of spinal muscular atrophy. Human Molecular Genetics *17*, 2552-2569.

Knippenberg,S., Thau,N., Dengler,R., and Petri,S. (2010). Significance of behavioural tests in a transgenic mouse model of amyotrophic lateral sclerosis (ALS). Behavioural Brain Research *213*, 82-87.

Li,H., Zhang,N., Lin,H., Yu,Y., Cai,Q.M., Li,H., Zhang,N., Lin,H., Yu,Y., and Cai,Q.M. (2014). Histological, cellular and behavioral assessments of stroke outcomes after photothrombosis-induced ischemia in adult mice. BMC Neuroscience *15*, 58.

Li,H., Xie,Y., Zhang,N., Yu,Y., Zhang,Q., and Ding,S. (2015). Disruption of IP_3R2-mediated Ca^{2+} signaling pathway in astrocytes ameliorates neuronal death and brain damage while reducing behavioral deficits after focal ischemic stroke. Cell Calcium *58*, 565-576.

Li,H., Zhang,N., Sun,G., and Ding,S. (2013). Inhibition of the group I mGluRs reduces acute brain damage and improves long-term histological outcomes after photothrombosis-induced ischaemia. ASN NEURO *5*.

Maeno-Hikichi,Y., Polo-Parada,L., Kastanenka,K.V., and Landmesser,L.T. (2011). Frequency-Dependent Modes of Synaptic Vesicle Endocytosis and Exocytosis at Adult Mouse Neuromuscular Junctions. The Journal of Neuroscience *31*, 1093-1105.

O'Leary,J.D., Kozareva,D.A., Hueston,C.M., O'Leary,O.F., Cryan,J.F., and Nolan,Y.M. (2016). The nuclear receptor Tlx regulates motor, cognitive and anxiety-related behaviours during adolescence and adulthood. Behavioural Brain Research *306*, 36-47.

Park,E.J., Sun,X., Nichol,P., Saijoh,Y., Martin,J.F., and Moon,A.M. (2008). System for tamoxifen-inducible expression of cre-recombinase from the Foxa2 locus in mice. Dev. Dyn. *237*, 447-453.

Polo-Parada,L., Bose,C.M., Plattner,F., and Landmesser,L.T. (2004). Distinct Roles of Different Neural Cell Adhesion Molecule (NCAM) Isoforms in Synaptic Maturation Revealed by Analysis of NCAM 180 kDa Isoform-Deficient Mice. The Journal of Neuroscience *24*, 1852-1864.

Polo-Parada,L., Plattner,F., Bose,C., and Landmesser,L.T. (2005). NCAM 180 Acting via a Conserved C-Terminal Domain and MLCK Is Essential for Effective Transmission with Repetitive Stimulation. Neuron *46*, 917-931.

Rongvaux,A., Galli,M., Denanglaire,S.+., Van Gool,F.d.r., Deze,P.L., Szpirer,C., Bureau,F., Andris,F., and Leo,O. (2008). Nicotinamide Phosphoribosyl Transferase/Pre-B Cell Colony-Enhancing Factor/Visfatin Is Required for Lymphocyte Development and Cellular Resistance to Genotoxic Stress. J Immunol *181*, 4685-4695.

Rooney,J.P., Ryde,I.T., Sanders,L.H., Howlett,E., Colton,M.D., Germ,K.E., Mayer,G.D., Greenamyre,J.T., and Meyer,J.N. (2015). PCR Based Determination of Mitochondrial DNA Copy Number in Multiple Species. In Mitochondrial Regulation: Methods and Protocols, C.M. Palmeira, and A.P. Rolo, eds. (New York, NY: Springer New York), pp. 23-38.

Schaar,K., Brenneman,M., and Savitz,S. (2010). Functional assessments in the rodent stroke model. Experimental & Translational Stroke Medicine *2*, 13.

Seijffers,R., Zhang,J., Matthews,J.C., Chen,A., Tamrazian,E., Babaniyi,O., Selig,M., Hynynen,M., Woolf,C.J., and Brown,R.H. (2014). ATF3 expression improves motor function in the ALS mouse model by promoting motor neuron survival and retaining muscle innervation. PNAS *111*, 1622-1627.

Tatem,K.S., Quinn,J.L., Phadke,A., Yu,Q., Gordish-Dressman,H., and Nagaraju,K. (2014). Behavioral and Locomotor Measurements Using an Open Field Activity Monitoring System for Skeletal Muscle Diseases. J Vis Exp. e51785.

Valdez,G., Tapia,J.C., Kang,H., Clemenson,G.D., Gage,F.H., Lichtman,J.W., and Sanes,J.R. (2010). Attenuation of age-related changes in mouse neuromuscular synapses by caloric restriction and exercise. PNAS *107*, 14863-14868.

Valdez,G., Tapia,J.C., Lichtman,J.W., Fox,M.A., and Sanes,J.R. (2012). Shared Resistance to Aging and ALS in Neuromuscular Junctions of Specific Muscles. PLoS ONE *7*, e34640.

Wang,X., Li,H., and Ding,S. (2014). The Effects of NAD^+ on Apoptotic Neuronal Death and Mitochondrial Biogenesis and Function after Glutamate Excitotoxicity. International Journal of Molecular Sciences *15*, 1012-1022.

Wang,X., Li,H., and Ding,S. (2016). Pre-B-cell colony-enhancing factor protects against apoptotic neuronal death and mitochondrial damage in ischemia. Scientific Reports *6*, 32416.

Wilkins,H.M., Koppel,S., Carl,S.M., Ramanujan,S., Weidling,I., Michaelis,M.L., Michaelis,E.K., and Swerdlow,R.H. (2016). Oxaloacetate enhances neuronal cell bioenergetic fluxes and infrastructure. Journal of Neurochemistry *137*, 76-87.

Wong,M., and Martin,L.J. (2010). Skeletal muscle-restricted expression of human SOD1 causes motor neuron degeneration in transgenic mice. Human Molecular Genetics *19*, 2284-2302.

Yang,K., Cheng,H., Gross,R.W., and Han,X. (2009). Automated lipid identification and quantification by multidimensional mass spectrometry-based shotgun lipidomics. Anal. Chem. *81*, 4356-4368.

Yang,K., and Han,X. (2011). Accurate Quantification of Lipid Species by Electrospray Ionization Mass Spectrometry-Meets a Key Challenge in Lipidomics. *1*.

Young,P., Qiu,L., Wang,D., Zhao,S., Gross,J., and Feng,G. (2008). Single-neuron labeling with inducible Cre-mediated knockout in transgenic mice. Nat Neurosci *11*, 721-728.

Zhang,W., Xie,Y., Wang,T., Bi,J., Li,H., Zhang,L.Q., Ye,S.Q., and Ding,S. (2010). Neuronal protective role of PBEF in a mouse model of cerebral ischemia. J Cereb Blood Flow Metab *30*, 1962-1971.